

# Multi – Mode Coupling of Protein Motion to Electron Transfer in the Photosynthetic Reaction Center: Spin – Boson Theory Based on a Classical Molecular Dynamics Simulation<sup>1</sup>

Dong Xu and Klaus Schulten\*

Beckman Institute and Department of Physics  
University of Illinois at Urbana-Champaign  
405 North Mathews Ave., Urbana, IL 61801, USA

## Abstract

We present a quantum mechanical description (spin–boson model) for electron transfer rates in the photosynthetic reaction center of *Rh. viridis* which assumes for the protein nuclear motion a broad distribution of vibrational modes rather than a few discrete modes. We demonstrate that linear coupling of electron transfer to such modes is in agreement with molecular dynamics simulations. We establish that the multi-mode coupling between electron transfer and protein motion can be described in surprisingly simple terms and requires as input only that one monitors the fluctuations of the so-called energy gap function  $\Delta E(t)$ , i.e., the energy required for a virtual transfer of the electron. The amplitude and the relaxation time of the associated correlation function are the essential parameters which determine electron transfer rates in the framework of the spin–boson model. We present the temperature and redox energy dependence of these rates which are found in agreement with observations and also with Marcus theory at high temperature, even though the latter assumes coupling to a single mode.

## 1 Introduction

The electron transfer in the photosynthetic reaction center of *Rh. viridis* involves three initial steps:  $P_S H_L Q_A Q_B \rightarrow P_S^+ H_L^- Q_A Q_B \rightarrow P_S^+ H_L Q_A^- Q_B \rightarrow P_S^+ H_L Q_A Q_B^-$ . Different from Arrhenius behavior of most chemical reactions, one observes that electron transfer rates vary little with temperature, in some instances even increase when temperature is lowered. In order to explain the redox and temperature dependence of electron transfer rates, previous interpretations have assumed that quantum mechanical behavior of electron transfer arises through a small number of nuclear degrees of freedom, such as one or two, particularly strongly coupled to the electron transfer reaction. In most cases, the respective theories can fit experiments very well, however, they rest on artificial parameters [2, 3, 4, 5, 6].

---

<sup>1</sup>Part of this paper is excerpt from [1]

The coupling between electron transfer and a protein as a medium is due to the Coulomb interaction, which is long range and encompasses a very large volume. Correspondingly, the coupling involves small, additive contributions of many motions of a protein rather than only a few dominant contributions. In fact, MD simulations reported in [7, 8, 9] revealed that the coupling involves essentially all nuclear degrees of freedom of the protein investigated, the photosynthetic reaction center. All components of the protein contribute rather evenly to the coupling between electron transfer and medium as simulations with and without cut-off of Coulomb interactions revealed.

One of the reasons why few-mode description of electron transfer in proteins are widely accepted is that it can be treated quantum mechanically, and that it fits experimental data over a wide temperature domain. In case of multi-mode coupling, one might be very discouraged by the fact that all degrees of freedom need to be described quantum mechanically, at least all those degrees of freedom for which holds  $k_B T \leq \hbar \omega_\alpha$  where  $\omega_\alpha$  is the frequency connected with the respective nuclear motion. However, in case one describes electron transfer as a 2-state process, assumes linear coupling as well as harmonic motion of the protein atoms, the resulting stochastic quantum system can be described in a rather straight forward way. Following earlier work by Onuchic et al. [10, 11, 12], we applied the spin–boson model to biological electron transfer[1]. We will demonstrate below that the resulting description is actually rather simple. The theory outlined employs classical simulations to obtain the relevant parameters. We will calculate the electron transfer rates as a function of redox energy and temperature [7].

## 2 Spin – Boson Model of Electron Transfer

A detailed review of the spin–boson model can be found in [13]. In case of electron transfer in proteins, the spin–boson model can be related to a simple microscopic picture, namely, the well-known Marcus energy diagram[14, 15]. In this diagram, the free energy of both reactant and product states is described by a one–dimensional harmonic potential with identical force constants  $f$ . We assume the reactant and product free energy curves have the functional form,

$$E_R = \frac{1}{2} f q^2, \quad E_P = \frac{1}{2} f (q - q_P)^2 - \epsilon_o. \quad (1)$$

In the above equations,  $q$  represents schematically the nuclear configuration of the protein and  $q_P$ ,  $\epsilon_o$  represent the shift of the equilibrium position after the electron transfer. As pointed out in [3] and [7], the potential functions originate from a dependence on thousands of nuclear coordinates, which define a many-dimensional potential-energy surface. The spin–boson model goes beyond the Marcus model in that it allows one to represent the multitude of degrees of freedom coupled to the electron transfer through an ensemble of harmonic oscillators of various frequencies. In analogy to Marcus theory, we also postulate that the nuclear degrees of freedom of the medium are too inert to change during the electron transfer step, i.e., the Born–Oppenheimer approximation can be applied for the nuclear degrees of freedom. Let

us assume that the protein matrix coupled to electron transfer can be represented through  $N$  different oscillators where  $N$  is of the order of magnitude of the number of atoms in the protein, i.e., about  $10^4$  in the case of the photosynthetic reaction center. We denote the frequencies of these oscillators by  $\omega_\alpha$ ,  $\alpha = 1, 2, \dots, N$  and the associated vibrational coordinates by  $q_\alpha$ ,  $\alpha = 1, 2, \dots, N$ . Let us assume further that each mode is coupled to the electron transfer such that the harmonic potentials in the reactant state ( $E_{R,\alpha}$ ) and in the product state ( $E_{P,\alpha}$ ) differ as follows ( $\alpha = 1, 2, \dots, N$ )

$$E_{R,\alpha} = \frac{1}{2} m_\alpha \omega_\alpha^2 q_\alpha^2, \quad E_{P,\alpha} = \frac{1}{2} m_\alpha \omega_\alpha^2 (q_\alpha - q_{o,\alpha})^2 - \epsilon_{o,\alpha}. \quad (2)$$

In this notation  $m_\alpha$  are effective constants which do not need to be individually identified as we will see below.

The total energy in the reactant and product states is then

$$E_R = \sum_{\alpha=1}^N \left( \frac{p_\alpha^2}{2m_\alpha} + E_{R,\alpha} \right), \quad E_P = \sum_{\alpha=1}^N \left( \frac{p_\alpha^2}{2m_\alpha} + E_{P,\alpha} \right), \quad (3)$$

where  $p_\alpha$  is the momentum operator of the oscillator. The spin–boson Hamiltonian combines these energies with a quantum mechanical 2-state Hamiltonian as follows

$$H_{sb} = \begin{pmatrix} E_R & V \\ V & E_P \end{pmatrix}, \quad (4)$$

where  $V$  accounts for the electron coupling between reactant and product states, the coupling originating from tunneling of the electron between electron donor and acceptor.

After some algebra [1], one can separate the above Hamiltonian into three parts and a constant  $C \mathbb{1}$

$$\hat{H}_{sb} = \hat{H}_{el} + \hat{H}_{osc} + \hat{H}_{coupl} + C \mathbb{1}. \quad (5)$$

The first term is a simple two–state Hamiltonian, resembling a spin operator

$$\hat{H}_{el} = V \sigma_x + \frac{1}{2} \epsilon \sigma_z, \quad (6)$$

where  $\sigma_x, \sigma_z$  are Pauli matrices.  $\epsilon$  accounts for the energy difference of reactant and product states and results from the sum of the redox energy of all modes

$$\epsilon = \sum_{\alpha=1}^N \epsilon_{o,\alpha}. \quad (7)$$

The second term in (5) represents the medium thermal motion described through an ensemble of independent linear oscillators (bosons)

$$\hat{H}_{osc} = \sum_{\alpha} \left( \frac{\hat{p}_\alpha^2}{2m_\alpha} + \frac{1}{2} m_\alpha \omega_\alpha^2 x_\alpha^2 \right) \mathbb{1} \quad (8)$$

where  $x_\alpha$  denotes the spatial coordinate

$$x_\alpha = q_\alpha - \frac{q_{o,\alpha}}{2}. \quad (9)$$

The third term in (5) represents the coupling between the vibrational degrees of freedom and the two-state system. The coupling is linear in  $x_\alpha$  and diagonal in the two-state system

$$\hat{H}_{coupl} = \frac{1}{2} \sigma_z \sum_\alpha c_\alpha x_\alpha. \quad (10)$$

Here  $c_\alpha$  describes the strength of the coupling of the electron transfer to the  $\alpha$ -th oscillator, in this case,

$$c_\alpha = m_\alpha \omega_\alpha^2 q_{o,\alpha}. \quad (11)$$

The last term in (5)

$$C \mathbb{1} = \frac{1}{2} \sum_{\alpha=1}^N \left( \epsilon_{o,\alpha} + \frac{1}{4} m_\alpha \omega_\alpha^2 q_{o,\alpha}^2 \right) \mathbb{1}, \quad (12)$$

is a constant which does not affect the electron transfer rates and, thus, can be omitted. The above derivation is not only a formal mathematical transformation, but also a shift from the multi-mode Marcus diagram to an equivalent physical picture, i.e., the spin-boson model.

Even though there appear many variables and parameters in the equations above, ultimately the spin-boson model, as advertised in [13], is characterized completely by a well defined average property of the system, the spectral function  $J(\omega)$

$$J(\omega) = \frac{\pi}{2} \sum_{\alpha=1}^N \frac{c_\alpha^2}{m_\alpha \omega_\alpha} \delta(\omega - \omega_\alpha). \quad (13)$$

$J(\omega)$  can be assumed to be a smooth function determined by few parameters. These parameters can be determined from a classical molecular dynamics simulation. Once one knows  $J(\omega)$  and  $V$ , one can calculate all the properties for the spin-boson system. As a matter of fact, the parameter  $V$  is not very important; it appears only in a pre-factor  $V^2$  which multiplies the electron transfer rate. The simple dependence results from an application of Fermi's golden rule, an approximation which appears to be valid in case of electron transfer [7].

### 3 The Relation between the Spin – Boson Model and Classical Molecular Dynamics Simulations

Previous investigations of the coupling of electron transfer and protein thermal motions have been based on classical descriptions (see [7] and references therein). The nuclear motions were complemented by a quantum mechanical description for the electron transfer, described by a 2-state model. The coupling to the classical protein motion yields a fluctuating diagonal contribution for the 2-state Hamiltonian as given

in (6). This contribution can be determined as the energy difference  $\Delta E(t)$  between reactant and product states at each instant in time. Figure 1 provides a good illustration how  $\Delta E(t)$  relates to the spin–boson model in the photosynthetic reaction center of *Rh. viridis*: the figure shows on the left hand side the protein atoms, rendered in grey, in which are embedded, rendered in black, the prosthetic groups involved in electron transfer: hemes, chlorophylls, pheophytines and quinones. The electron transfer is coupled to a wide range of protein atoms through long range Coulomb forces. The right hand side indicate one of the electron transfer reactions;  $\Delta E(t)$  represents the energy gap between reactant and product states which strongly fluctuates due to the coupling to the thermal motion of the protein. The two states of electron transfer are described as the spin operator [see Eq. (6)], while the thermal vibrations of the protein correspond to the bosons in the spin–boson model.

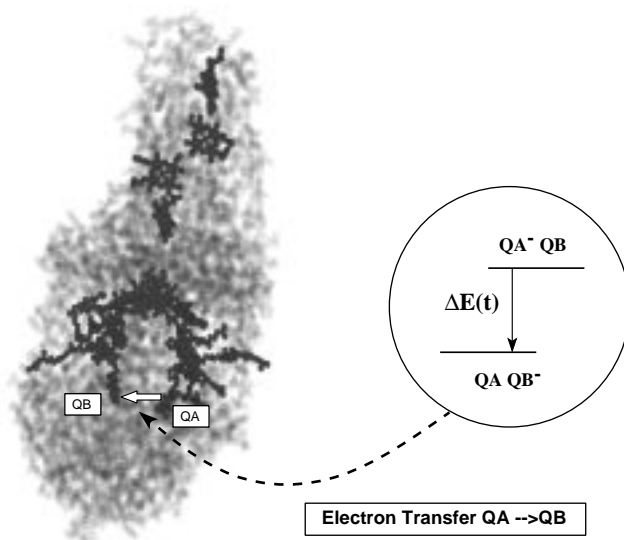


Figure 1: This figure shows on the left hand side the protein atoms of the photosynthetic reaction center of *Rhodospseudomonas viridis* (in grey) and the prosthetic groups involved in electron transport (in black). One can recognize in the upper part of the protein complex four heme groups. The center contains a sandwich complex of two chlorophylls from which stretch to both sides each a chlorophyll, a pheophytine and, towards the bottom, a quinone. These prosthetic groups conduct electrons, the electron movement being accompanied by a response of the thermal motion of the (grey) protein atoms. Indicated is also on the right hand side one of the electron transfer reactions,  $Q_A \rightarrow Q_B$ ;  $\Delta E(t)$  represents the energy gap between reactant and product states which depends strongly on the thermal motion of the protein. In the spin–boson model, the two states of electron transfer are described as the spin operator, while thermal vibrations of the protein are accounted for by the boson operators.

As long as one can assume that the Hamiltonian is temperature independent, e.g., that the protein structure and, hence, the coupling terms as well as the spectral function  $J(\omega)$  do not change with temperature, one can expect that the classical simulations allow one to determine a suitable quantum mechanical model. For this

purpose, one carries out a classical simulation at high temperature, characterizes  $J(\omega)$  corresponding to the simulated  $\Delta E(t)$  and employs the the resulting  $J(\omega)$  at all temperatures. Since at physiological temperatures ( $T = 300$  K), the majority of frequencies of modes satisfy the property  $\hbar\omega_\alpha/k_B T \ll 1$  one can assume the classical limit to be realized at  $T = 300$  K. At this temperatures, quantum descriptions and classical descriptions should then coincide and, therefore, the classical simulations should allow one to determine a suitable characteristic function  $J(\omega)$ .

$J(\omega)$  in the spin–boson system can be characterized in molecular dynamics simulations through the energy–energy correlation function, as discussed in [7, 8]:

$$C(t) = \langle (\Delta E(t) - \langle \Delta E \rangle) (\Delta E(0) - \langle \Delta E \rangle) \rangle, \quad (14)$$

$J(\omega)$  and  $C(t)$  are related to each other through the Fourier cosine transform. It holds [1, 16, 17]

$$\frac{J(\omega)}{\omega} = \frac{1}{k_B T} \int_0^\infty dt C(t) \cos \omega t, \quad (15)$$

$$C(t) = \frac{2k_B T}{\pi} \int_0^\infty d\omega \frac{J(\omega)}{\omega} \cos \omega t. \quad (16)$$

If one monitors in a classical MD simulation, the normalized correlation function, i.e.,  $C_1(t) = C(t)/C(0)$ , and the rms-deviation from the mean of  $\Delta E(t)$  i.e.,

$$\sigma = \sqrt{\langle \Delta E^2 \rangle - \langle \Delta E \rangle^2}, \quad (17)$$

then one can use the following expression [1] to determine  $J(\omega)$

$$\frac{J(\omega)}{\omega} = \frac{\sigma^2}{k_B T} \int_0^\infty dt C_1(t) \cos \omega t. \quad (18)$$

In the simulations reported in [7] for the electron transfer  $P_S \rightarrow H_L$ ,  $C_1(t)$  exhibits an approximate exponential decay with a relaxation time  $\tau = 94$  fs. The simulation in [7] also provided  $\sigma = 3.9$  kcal/mol at a temperature  $T = 300$  K. For the sake of simplicity we will assume that the energy–energy correlation function is well represented by a mono-exponential function  $e^{-\frac{t}{\tau}}$ . The relationship (18) then yields

$$J(\omega) = \frac{\sigma^2 \omega}{k_B T} \int_0^\infty dt e^{-t/\tau} \cos \omega t = \frac{\eta \omega}{1 + \omega^2 \tau^2}; \quad (19)$$

$$\eta = \frac{\sigma^2 \tau}{k_B T} = 25.15 h. \quad (20)$$

where  $h$  is Planck’s constant.

## 4 Calculation of Electron Transfer Rates

In order to determine the electron transfer rate  $k(\epsilon, T)$ , we start from the expression provided in [13]

$$k(\epsilon, T) = \left( \frac{2V}{\hbar} \right)^2 \int_0^\infty dt \cos \left( \frac{\epsilon t}{\hbar} \right) \cos \left[ \frac{Q_1(t)}{\pi \hbar} \right] \exp \left[ -\frac{Q_2(t)}{\pi \hbar} \right]. \quad (21)$$

Evaluation of this expression requires first an evaluation of the time-dependent functions  $Q_1(t)$  and  $Q_2(t)$  which are defined in terms of integrals over  $J(\omega)$  as follows

$$\begin{aligned} Q_1(t) &= \int_0^\infty d\omega \omega^{-2} J(\omega) \sin \omega t \\ Q_2(t) &= 2 \int_0^\infty d\omega \omega^{-2} \sin^2 \left( \frac{\omega t}{2} \right) \coth \left( \frac{\beta \hbar \omega}{2} \right) J(\omega) \end{aligned} \quad (22)$$

where  $\beta = 1/k_B T$ . Using the expression (19) for  $J(\omega)$  one obtains  $Q_1(t)$  analytically

$$Q_1(t) = \int_0^\infty d\omega \frac{\eta \sin \omega t}{\omega (1 + \omega^2 \tau^2)} = \frac{\eta \pi}{2} \left[ 1 - \exp \left( -\frac{t}{\tau} \right) \right] \quad (23)$$

The electron transfer rate is then

$$\begin{aligned} k(\epsilon, T) &= \left( \frac{2V}{\hbar} \right)^2 \int_0^\infty dt \cos \left( \frac{\epsilon t}{\hbar} \right) \cos \left[ \frac{\eta}{2\hbar} (1 - e^{-t/\tau}) \right] \times \\ &\times \exp \left[ -\frac{2\eta}{\pi \hbar} \int_0^\infty d\omega \frac{\sin^2 \left( \frac{\omega t}{2} \right)}{\omega (1 + \omega^2 \tau^2)} \coth \left( \frac{\beta \hbar \omega}{2} \right) \right]. \end{aligned} \quad (24)$$

To simplify this expression we define  $x = t/\tau$ ,  $y = \omega\tau$ , and  $\gamma = \eta/h$ . This yields the final expression

$$\begin{aligned} k(\epsilon, T) &= \left( \frac{2V}{\hbar} \right)^2 \tau \int_0^\infty dx \cos \left( \frac{\epsilon \tau}{\hbar} x \right) \cos \left[ \gamma \pi (1 - e^{-x}) \right] \times \\ &\times \exp \left[ -4\gamma \int_0^\infty dy \frac{\sin^2 \left( \frac{xy}{2} \right)}{y (1 + y^2)} \coth \left( \frac{\hbar}{2k_B \tau} \cdot \frac{y}{T} \right) \right]. \end{aligned} \quad (25)$$

The stated numerical values of  $V/\hbar$  in [7] is  $5 \text{ ps}^{-1}$ . Equations (25) allow one, in principle, to evaluate the electron transfer rate  $k(\epsilon, T)$ . However, straightforward numerical quadrature of (25) is very time consuming since it involves a double integral. One can use some faster, albeit approximate expressions for the  $\exp[\dots]$  factor in the integrand of (25). We define

$$q_2(x) = \int_0^\infty dy \frac{\sin^2 \left( \frac{xy}{2} \right)}{y (1 + y^2)} \coth(\alpha y), \quad \alpha = \frac{\hbar}{2k_B \tau T}. \quad (26)$$

As demonstrated in [1],  $q_2(x)$  is a monotonously increasing function of  $x$ . Hence the main contribution to (25) stems from the region of small  $x$ . When  $x$  is small, there are at least two ways to approximate  $q_2(x)$  in a very simple form. One is to calculate some sample points at small  $x$  and at a certain temperature for  $q_2(x)$ , and then fit all the points into the form  $Ax^\delta$  with  $1 < \delta < 2$ . The other way, suggested by A. Szabo (private communication), is based on the analytical expansion of  $q_2(x)$  which holds for small  $x$

$$q_2(x) \approx \frac{x^2}{4} [f(\alpha) - \ln x] \quad (27)$$

where

$$f(\alpha) = \int_0^\infty \frac{y dy}{1 + y^2} (\coth(\alpha y) - 1). \quad (28)$$

The second approach is very useful to derive further approximate properties for  $k(\epsilon, T)$ .

Since  $q_2(x)$  is  $\epsilon$ -independent one can use the same numerical approximation for all  $\epsilon$  values considered. Hence, for a given temperature obtaining  $k(\epsilon, T)$  at all different  $\epsilon$  values requires one to evaluate  $q_2(x)$  only once. Then (25) becomes

$$k_{appr}(\epsilon, T) = \left(\frac{2V}{\hbar}\right)^2 \tau \int_0^\infty dx \cos\left(\frac{\epsilon\tau}{\hbar} x\right) \cos\left[\gamma\pi(1 - e^{-x})\right] e^{-4\gamma q_2(x)}. \quad (29)$$

Obviously, the numerical procedure chosen is much less time consuming than evaluating (25) by double quadrature.

## 5 High and Low Temperature Limit

### 5.1 High Temperature Limit

The expression (21) of the electron transfer rate together with the functional behavior of  $Q_2(t)$  suggests that one may employ the method of steepest descent, at least in the high temperature limit, for an approximate evaluation. This approximation is based on a quadratic expansion of  $Q_2(t)$  around its minimum at  $t = 0$ . The procedure requires one to determine the quantity

$$\mu = \left. \frac{d^2}{dt^2} Q_2(t) \right|_{t=0} \quad (30)$$

The expression for  $Q_2(t)$  in (22) yields

$$\mu = \int_0^\infty d\omega J(\omega) \coth\left(\frac{\beta\hbar\omega}{2}\right). \quad (31)$$

Unfortunately, for many choices of  $J(\omega)$  this expression diverges and the steepest descent method cannot be applied. However, we note that the divergence of (31) is due to  $\omega \rightarrow \infty$  contributions to the integral over  $J(\omega)$ . Since the number of modes in a protein are finite, the divergence in (31) is due to an artificial analytical form of  $J(\omega)$ . If one would assume a cut-off frequency  $\omega_c$ , i.e., replace  $J(\omega)$  by  $J(\omega)\theta(\omega - \omega_c)$ , a divergence would not arise in (31). One may, hence, assume that the second derivative (30) actually exists, approximate

$$Q_2(t) \approx \frac{1}{2} \mu t^2, \quad (32)$$

and employ this in a steepest descent method.

At a sufficiently high temperature, contributions to the integral in (21) arise only in a vicinity of  $t = 0$  in which (32) is small. In this case, one can approximate  $Q_1(t)$  in (22) linearly around  $t = 0$

$$Q_1(t) \approx \nu t; \quad \nu = \left. \frac{d}{dt} Q_1(t) \right|_{t=0} \quad (33)$$

where

$$\nu = \int_0^\infty d\omega \frac{J(\omega)}{\omega}. \quad (34)$$

By using the approximations (32) and (33) in (21), if  $\epsilon$  is not close to 0, one obtains [10, 11, 1]

$$k(\epsilon, T) \approx \frac{2\pi V^2}{\hbar} \frac{1}{\sqrt{2\pi\delta^2}} \exp\left[-\frac{(\epsilon - \epsilon_m)^2}{2\delta^2}\right]. \quad (35)$$

where

$$\delta^2 = \frac{\hbar\mu}{\pi} = \frac{\hbar}{\pi} \int_0^\infty d\omega J(\omega) \coth\left(\frac{\beta\hbar\omega}{2}\right) \quad (36)$$

$$\epsilon_m = \frac{\nu}{\pi} = \frac{1}{\pi} \int_0^\infty d\omega \frac{J(\omega)}{\omega}. \quad (37)$$

At a high enough temperature, i.e.,  $T > 100$  K, according to our numerical calculations, one can show further [1]

$$\delta = \sigma; \quad \epsilon_m = \frac{\sigma^2}{2k_B T}. \quad (38)$$

According to (37),  $\epsilon_m$  is actually temperature independent. Hence, one can rewrite (35) into a form which agrees with the rate predicted by the classical Marcus theory

$$k_M(\epsilon, T) = \frac{2\pi V^2}{\hbar} \frac{1}{\sqrt{2\pi f k_B T q_o^2}} \exp\left[-\frac{(\epsilon - \frac{1}{2} f q_o^2)^2}{2k_B T f q_o^2}\right] \quad (39)$$

where

$$f q_o^2 = 2\epsilon_m = \left. \frac{\sigma^2}{k_B T} \right|_{T=300K}. \quad (40)$$

## 5.2 Low Temperature Limit

At low temperatures, one can employ (28) for  $\alpha = \frac{\hbar}{2k_B \tau T} \rightarrow \infty$ , to approximate  $q_2(x)$  further. It can be verified

$$\lim_{\alpha \rightarrow \infty} f(\alpha) = \frac{\pi^2}{12\alpha^2}. \quad (41)$$

The value of the integral in (29) results mainly from contribution of small  $x$ , Accordingly at low temperatures, we can assume the overall integrand to be dominated by

the interval in which  $\gamma\pi^2x^2/12\alpha^2$  is small. Therefore, one can apply (27) to expand the exponential part of (29),

$$\begin{aligned} e^{-4\gamma q_2(x)} &= \exp\left(\gamma x^2 \ln x - \frac{\gamma\pi^2 x^2}{12\alpha^2}\right) \\ &= \exp(\gamma x^2 \ln x) \left[1 - \left(\frac{\gamma\pi^2 x^2}{12}\right) \left(\frac{2k_B\tau T}{\hbar}\right)^2\right]. \end{aligned} \quad (42)$$

Then the electron transfer rate at  $T \rightarrow 0$  can be expressed

$$k(\epsilon, T) \approx k(\epsilon, 0) - k_1(\epsilon) \left(\frac{2k_B\tau T}{\hbar}\right)^2, \quad (43)$$

where

$$k_1(\epsilon) = \left(\frac{2V}{\hbar}\right)^2 \tau \int_0^\infty dx \cos\left(\frac{\epsilon\tau}{\hbar} x\right) \cos\left[\gamma\pi(1 - e^{-x})\right] \left(-\frac{\gamma\pi^2 x^2}{12}\right) \exp(\gamma x^2 \ln x). \quad (44)$$

From (43), one concludes that at low temperatures, the electron transfer rate is actually changing very slowly. This behavior has been found in many observations [5, 18].

## 6 Results

In Figure 2 we present the calculated electron transfer rates  $k(\epsilon)$  as a function of the redox energy difference  $\epsilon$  for temperatures  $T = 10$  K and  $T = 300$  K, and compare the results to transfer rates predicted by the Marcus theory. One can observe that at high temperatures, the rate evaluated from the Marcus theory in a wide range of  $\epsilon$  agrees well with those evaluated from the spin-boson model at  $T = 300$  K, a behavior which is expected from the high temperature limit derived above. However the Marcus theory and the spin-boson model differ significantly at  $T = 10$  K. The rate as a function of  $\epsilon$  at low temperatures for the spin-boson model is asymmetrical. This result agrees with observations reported in [6] which show a distinct asymmetry with respect to  $\epsilon_m$  at low temperatures. Such asymmetry is not predicted by the models of Marcus and Hopfield [3, 4, 2].

If one makes the assumption that biological electron transfer systems evolved their  $\epsilon$ -values such that rates are optimized, one should expect that electron transfer rates in the photosynthetic reaction center are formed through a choice of  $\epsilon \rightarrow \epsilon_{max}$ , such that  $k(\epsilon_{max})$  is a maximum. In Fig. 3 we present corresponding maximum transfer rates,  $k(\epsilon_{max})$  as well as non-optimal values for  $\epsilon = \epsilon_{max} \pm \delta$ , where  $\delta = 2.5$  kcal/mol. Experimental data of electron transfer processes in the photosynthetic reaction center show increases similarly to those presented in Fig. 3 [19, 20, 21, 18]. However, Figure 3 demonstrates also that electron transfer at  $\epsilon$ -values slightly off the maximum position can yield a different temperature dependence than that of  $k(\epsilon_{max}, T)$ , namely temperature independence or a slight decrease of the rate with

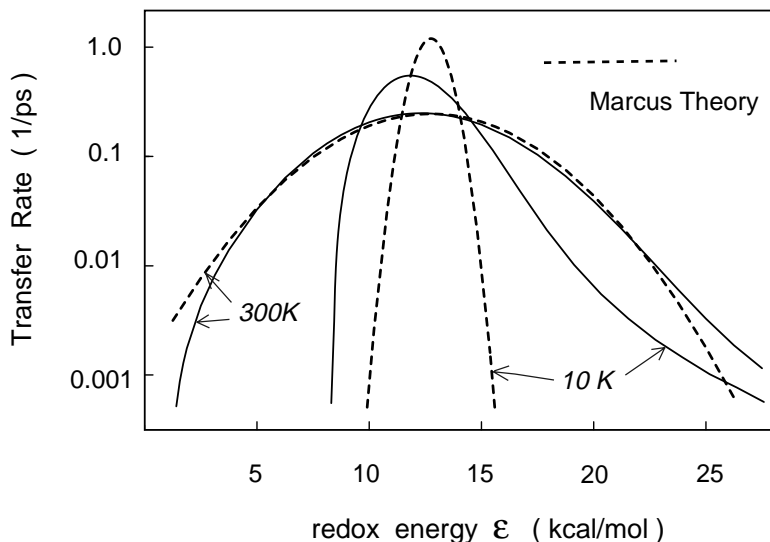


Figure 2: Comparison of electron transfer rates  $k(\epsilon, T)$  shown as a function of  $\epsilon$  evaluated in the framework of the spin-boson model (solid lines) and by Marcus theory (dashed lines) at temperatures 10 K and 300 K. The functions are centered approximately around  $\epsilon_m$ .

decreasing temperature. Such temperature dependence has also been observed for biological electron transfer [18]. As Nagarajan et al. reported in [18] the temperature dependence of the transfer rate resembles that of  $k(\epsilon_{max}, T)$  in photosynthetic reaction centers of native bacteria and in (M)Y210F mutants with tyrosine at the 210 position of the M-unit replaced by phenylalanine. However, a replacement of this tyrosine by isoleucine ((M)Y210I-mutant) yields a transfer rate which decreases like  $k(\epsilon_{max} - \delta, T)$  shown in Fig. 3. This altered temperature dependence should be attributed to a shift of the redox potentials, i.e.,  $\epsilon_{max} \rightarrow \epsilon_{max} - \delta$ .

## 7 Summary

The key new aspect of our investigation is two-fold: first, we base all model parameters on molecular dynamics simulations; second, the spin-boson model allows one to account for a very large number of vibrations quantum mechanically. We have demonstrated that the spin-boson model is well suited to describe the coupling between protein motion and electron transfer in biological redox systems. The model, through the spectral function  $J(\omega)$ , can be matched to correlation functions of the redox energy differences  $\Delta E(t)$  through the relationships (15, 18) where  $\Delta E(t)$  can be determined through a classical molecular dynamics simulation. We have demonstrated that the expressions for the electron transfer rates resulting from the spin-boson model can be evaluated numerically for a wide range of redox energy differences  $\epsilon$  and temperatures  $T$ . The input parameters involved in the calculations are from molecular simulations rather than from an artificial fit. Hence even though the spin-boson model may not yield qualitatively different predictions from models involving a small number of vibrational modes coupled to the electron transfer, it certainly

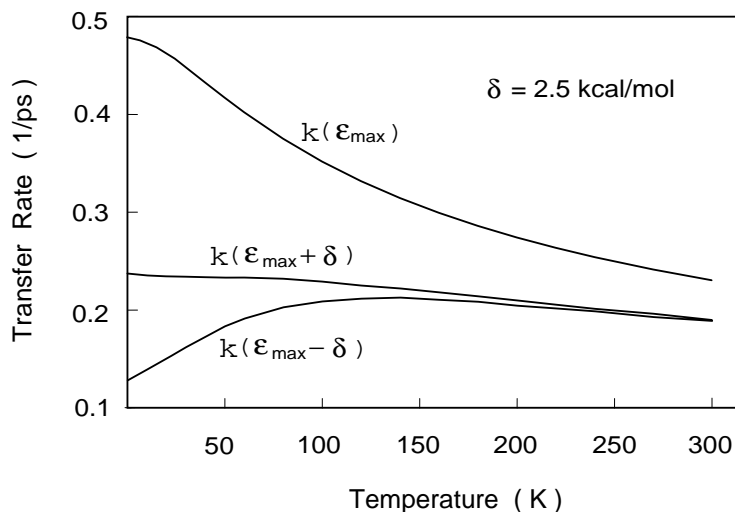


Figure 3: Comparison of the temperature dependence of the maximum transfer rate of  $k(\epsilon_{max})$  and off-maximum value  $k(\epsilon_{max} \pm \delta)$ , where  $\delta = 2.5$  kcal/mol.  $k(\epsilon_{max}, T)$  represents the fastest transfer rate of the system, the rates  $k(\epsilon_{max} \pm \delta, T)$  are slower since their  $\epsilon$ -values deviate from the optimal value  $\epsilon_{max}$ .

makes the role of the medium surrounding an electron transfer reaction appear in a new light: essentially all medium motions are coupled significantly to the reaction. The main result regarding the electron transfer rates evaluated is that for a spectral function consistent with molecular dynamics simulations the spin-boson model at physiological temperatures predicts transfer rates in close agreement with those predicted by the Marcus theory. However, at low temperatures deviations from the Marcus theory arise. The resulting low temperature rates are in qualitative agreement with observations. The spin-boson model explains, in particular, in a very simple and natural way the slow rise of transfer rates with decreasing temperature, as well as the asymmetric dependence of the redox energy.

The combination of simulation methods and analytical theory has proven to be a promising approach to investigate biological redox processes. Neither approach by itself can be successful since, on the one hand, proteins are too heterogeneous and ill understood to be molded into simple models, on the other hand, simulation methods are blind, leaving one with too much information and as a result, with none. The present example, connecting a single simulated observable, the medium redox energy contribution  $\Delta E(t)$ , with a model, the spin-boson model, which does not contain superfluous or undetermined parameters, most likely can be extended to other important protein reactions.

## Acknowledgements

We thank A. Leggett for directing us towards the spin-boson model and for helpful advice. We are also grateful to A. Szabo for pointing out the analytical approximation for  $q_2(x)$ . This work has been supported by the National Institutes of Health

(grant P41-RR05969). Computer time for this project has been made available by the National Center for Supercomputing Applications funded by the National Science Foundation.

## References

- [1] Dong Xu and Klaus Schulten. Coupling of protein motion to electron transfer in a photosynthetic reaction center: Investigating the low temperature behaviour in the framework of the spin-boson model. *Chem. Phys.*, 1991. submitted.
- [2] J. J. Hopfield. Electron transfer between biological molecules by thermally activated tunneling. *Proc. Natl. Acad. Sci. USA*, 71:3640–3644, 1974.
- [3] R. A. Marcus and N. Sutin. Electron transfers in chemistry and biology. *Biochem. Biophys. Acta*, 811:265–322, 1985.
- [4] H. Sumi and R. A. Marcus. Dynamical effects in electron transfer reactions. *J. Chem. Phys.*, 84:4894–4914, 1986.
- [5] G. R. Fleming, J. L. Martin, and J. Breton. Rate of primary electron transfer in photosynthetic reaction centers and their mechanistic implications. *Nature.*, 333:190–192, 1988.
- [6] M. R. Gunner and P. Leslie Dutton. Temperature and  $\Delta G_o$  dependence of the electron transfer from  $BPh^-$  to  $Q_a$  in a reaction center protein from *rhodobacter sphaeroides* with different quinones as  $Q_a$ . *J. Am. Chem. Soc.*, 111:3400–3412, 1989.
- [7] K. Schulten and M. Tesch. Coupling of bulk atomic motion to electron transfer: Molecular dynamics and stochastic quantum mechanics study of photosynthetic reaction centers. *Chemical Physics*, 158:421–446, 1991.
- [8] M. Nonella and K. Schulten. Molecular dynamics simulation of electron transfer in proteins — theory and application to  $Q_A \rightarrow Q_B$  transfer in the photosynthetic reaction center. *J. Phys. Chem.*, 95:2059–2067, 1990.
- [9] Herbert Treutlein, Klaus Schulten, J. Deisenhofer, H. Michel, Axel Brünger, and Martin Karplus. Chromophore-protein interactions and the function of the photosynthetic reaction center: A molecular dynamics study. *Proc. Natl. Acad. Sci. USA*, 89:75–79, 1991.
- [10] A. Garg, J. N. Onuchic, and V. Ambegaokar. Effect of friction on electron transfer in biomolecules. *J. Chem. Phys.*, 83:4491–4503, 1985.

- [11] J. N. Onuchic, D. N. Beratan, and J. J. Hopfield. Some aspects of electron-transfer reaction dynamics. *J. Phys. Chem.*, 90:3707–3721, 1986.
- [12] J. N. Onuchic. Effect of friction on electron transfer: The two reaction coordinate case. *J. Chem. Phys.*, 86:3925–3943, 1987.
- [13] A. J. Leggett, S. Chakravarty, A. T. Dorsey, M. P. A. Fisher, A. Garg, and W. Zwerger. Dynamics of the dissipative two-state system. *Rev. Mod. Phys.*, 59:1–85, 1985.
- [14] R. A. Marcus. On the energy of oxidation-reduction reactions involving electron transfer. I. *J. Chem. Phys.*, 24:966–978, 1956.
- [15] R. A. Marcus. Electrostatic free energy and other properties of states having nonequilibrium polarization. II. *J. Chem. Phys.*, 24:979–989, 1956.
- [16] Ilya Rips and Joshua Jortner. Dynamic solvent effects on outer-sphere electron transfer. *J. Chem. Phys.*, 87:2090–2104, 1987.
- [17] J. S. Bader and D. Chandler. Computer simulation of photochemically induced electron transfer. *Chem. Phys. Lett.*, 157:501–504, 1989.
- [18] V. Nagarajan, W. W. Parson, D. Gaul, and C. Schenck. Effect of specific mutations of tyrosine-(m)210 on the primary photosynthetic electron-transfer process in rhodobacter sphaeroides. *Proc. Natl. Acad. Sci. USA*, 87:7888–7892, 1990.
- [19] M. Bixon and J. Jortner. Coupling of protein modes to electron transfer in bacterial photosynthesis. *J. Phys. Chem.*, 90:3795–3800, 1986.
- [20] J. L. Martin, J. Breton, J. C. Lambry, and G. Fleming. The primary electron transfer in photosynthetic purple bacteria: Long range electron transfer in the femtosecond domain at low temperature. In J. Breton and A. Vermeglio, editors, *The Photosynthetic Bacterial Reaction Center: Structure and Dynamics*, pages 195–203, New York and London, 1988. Plenum Press.
- [21] C. Kirmaier and D. Holten. Temperature effects on the ground state absorption spectra and electron transfer kinetics of bacterial reaction centers. In J. Breton and A. Vermeglio, editors, *The Photosynthetic Bacterial Reaction Center: Structure and Dynamics*, pages 219–228, New York and London, 1988. Plenum Press.